Landslide Detection Using Densely Connected Convolutional Networks and Environmental Conditions

Haojie Cai, Tao Chen, *Senior Member, IEEE*, Ruiqing Niu, and Antonio Plaza, *Fellow, IEEE*

***Abstract*—A complete and accurate landslide map is necessary for landslide susceptibility and risk assessment. Currently, deep learning faces the dilemma of insufficient application, scarce samples, and poor efficiency in landslide recognition. This article utilizes the advantages of dense convolutional networks (DenseNets) and their modified technique to solve the three proposed problems. For this purpose, we created a new landslide sample library. On the original remote sensing image, 12 geological, topographic, hydrological and land cover factors that can directly or indirectly reflect the landslide are superimposed. Then, landslide detection was carried out in the three Gorges reservoir area in China to test the performance of the improved method. The quantitative evaluation of the landslide detection map shows that the combination of environmental factors and DenseNet can improve the accuracy of the detection model. Compared with the optical image, kappa and F1 increased by 9.7% and 9.1% respectively. Compared with other traditional neural networks and machine learning algorithms, DenseNet has the highest kappa and F1 values. Based on the base Densenet, through data augmentation and fine-tuning optimization technology, the kappa and F1 values reach the highest values of 0.9474 and 0.9505, respectively. The proposed method has promising applicability in large area landslide identification scenarios.**

***Index Terms*—Dense convolutional networks, image classification, landslide detection.**

I. Introduction

LANDSLIDE refers to the slip phenomenon of slope rock soil along the through shear plane, which is caused by human activity and environmental conditions [1]. Landslide geological disasters often cause environmental disruptions, casualties, and severe threats to human life and property [2]. The three Gorges reservoir in China is a world-renowned concentrated distribution area of reservoir bank landslides. According to statistics, there are a total of 428 landslides with a single scale exceeding 1.0 × 105 m3. Since the Three Gorges Dam was constructed and impounded, these numbers are still increasing [3]. For instance, the Xiling Gorge Xintan landslide destroyed the Millennium Old Town in Xintan, destroyed 481 residential houses, caused a surge of 54 m in height, affected 42 km of the Yangtze River Channel, and suspended shipping for 12 days [4]. The Jipazi landslide destroyed 1730 houses and caused an economic loss of approximately 6 million yuan, which caused a seven-day shipping interruption. To understand the causes and control factors of these landslides, and to react to variation tendencies in space and long time series, identifying existing landslides and making detailed landslide map libraries for model development and evaluation are valuable [5], [6].

Traditional method of landslide detection and mapping is field surveys, which belong to the geomorphological analysis of the research area [7]. This method has difficulty identifying old landslides [7]. In addition, because the field of view is limited by the slope, the ability of field investigations to accurately grasp the boundary information of landslides is limited [7], [8]. The purpose of field landslide investigation is detection and mapping landslide areas caused by specific events, such as earthquakes and rainfall, and observation and identification of landslide type and characteristics to provide a basis for the interpretation of satellite or aerial images [9]. Field surveys are difficult to access in many places and slow in efficiency. With the rapid development of earth observation technology, disaster emergency warning and regional mapping applications are also combined with remote sensing. Remote sensing has the characteristics of being fast, macroscale, and all-weather, and can quickly obtain macrosurface information [10]. At the same time, the improvement of remote sensing image time, spectrum and spatial resolution provides a robust database for remote sensing applications [11], [12]. Utilizing remote sensing technology to monitor and govern landslides has the advantages of economy and speed. Remote sensing is widely used in landslide detection or investigation, monitoring, and susceptibility analysis [13]–[15]. The original method of extracting landslide information from remote sensing images was visual

Manuscript received October 18, 2020; revised February 3, 2021 and April 27, 2021; accepted May 1, 2021. Date of publication May 11, 2021; date of current version May 31, 2021. This work was supported in part by the National Natural Science Foundation of China under Grant 62071439, Grant 61601418, and Grant 61871259, in part by the Opening Foundation of Qilian Mountain National Park Research Center (Qinghai) under Grant GKQ2019-01, in part by the Opening Foundation of Beijing Key Laboratory of Urban Spatial Information Engineering, under Grant 20210209, and in part by the Opening Foundation of Geomatics Technology and Application Key Laboratory of Qinghai Province, under Grant QHDX-2019-01. (*Corresponding author: Tao Chen.*)

Haojie Cai and Ruiqing Niu are with the Institute of Geophysics and Geomatics, China University of Geosciences, Wuhan 430074, China (e-mail: cason@cug.edu.cn; niuruiqing@cug.edu.cn).

Tao Chen is with the Institute of Geophysics and Geomatics, China University of Geosciences, Wuhan 430074, China, and also with the Beijing Key Laboratory of Urban Spatial Information Engineering, Beijing 100038, China (e-mail: taochen@cug.edu.cn).

Antonio Plaza is with the Hyperspectral Computing Laboratory, Department of Technology of Computers and Communications, Escuela Politécnica, University of Extremadura, 10071 Cáceres, Spain (e-mail: aplaza@unex.es).

Digital Object Identifier 10.1109/JSTARS.2021.3079196

interpretation, and has achieved good results in landslides, debris flows, and other geological disasters. Visual interpretation is a method of landslide detection based on image hue, texture, shape, position, and mutual relationship [16]. The interpretation mark of landslides mainly comes from the spectral, geometric and texture features of the landslide body shown on remote sensing images, and then these marks and geological knowledge are analyzed by visual observation and combination with other nonremote sensing data [16], [17]. For example, landslides can cause extensive damage to vegetation, and further expose rocks and soil on the surface, thereby increasing the brightness of the image. Image brightness features are of great significance to the identification of landslide areas [18]. However, visual interpretation is too dependent on the interpreter's experience and knowledge ability, and the workload is heavy, the work cycle is long, it is difficult to meet emergency needs, and the results are sometimes unreliable [19].

To improve the efficiency and precision of landslide detection, many computer interpretation methods are used for remote sensing geoscience information extraction tasks. Computer interpretation is the comprehensive application of geoscience analysis, remote sensing image processing, geographic information systems, pattern recognition, and artificial intelligence technology with the support of computer systems to realize the intelligent acquisition of geoscience topic information [20]. The computer interpretation methods applied to landslides can be divided into statistics-based and heuristic methods. Statistical methods include the weight of evidence, logistic regression, and analytic hierarchy process; when new methods are implemented, they can be used as benchmark methods [21]. Heuristic methods or machine learning (ML) methods tend to use advanced algorithms to establish relationships by analyzing the relationship between landslide and nonlandslide features. The ML method is an automatic modeling method for analyzing data. It can learn the basic relationships existing in the data to build an analysis model. They can produce accurate and repeatable results by an iterative learning process [21]. Currently, the popular ML algorithms applied to landslide susceptibility analysis, identification and monitoring are support vector machines (SVMs) [22], [23], random forests (RFs) [24], rotation forests [25], and ensemble learning including bagging [26]. Traditionally, remote sensing image interpretation combined with ML uses statistical methods such as maximum likelihood and k-means clustering depending on spectral and texture features [11]. These methods are based on pixels. The pixel-based landslide extraction method ignores the context of landslides. In fact, landslides have other attributes (shape, texture, spatial structure, mutual relationship, etc.). In recent years, methods such as object-oriented analysis, artificial neural networks, genetic algorithms, and SVMs have achieved good results [11], [27]. The object-oriented method fully considers the characteristics of the landslide, which reduces the error of extracting information from only pixels and obtains higher accuracy [28], [29]. However, object-oriented methods require image segmentation first, and the quality of the segmentation scale determines the landslide detection result [7]. Complex, large-scale remote sensing images complicate the segmentation process, resulting in low-efficiency landslide detection [30]. Whether it is based on pixels or objects, these ML methods require the design of interpretation logic or the extraction of features in the image, which leads to complex algorithm design and limits the potential for algorithm improvement [11], [27].

In recent years, with the improvement of computer computing power, the development of deep learning has experienced new peaks. Deep learning has made great achievements in many applications, such as image classification [31], object detection [32], [33], and natural language processing [34]. Influenced by these successful applications, deep learning methods based on pixels and objects have been proposed for landslide detection and susceptibility [35]–[37]. In the deep learning model, convolutional neural networks (CNNs) are the core module. The convolution kernel of CNNs can automatically obtain an effective feature representation of the image, which allows CNNs to understand the object semantic information without the need to manually design complex features [38]. Although the performance of CNNs has been greatly improved and many real-world problems have been solved, only a few studies have introduced CNNs into remote sensing images for landslide detection [39]–[42]. Sameen *et al*. improved CNN using residual blocks, and applied modified CNN to aerial photography and LiDAR data for landslide detection [43]. Yu *et al*. dealt with the problem of sample imbalance in landslide detection by a modified pyramid scene parsing network (PSPNet) [44]. Their modified PSPNet achieved an F1 score of 0.88. Although it is not the first time that CNNs have been used for landslide detection, there are still the following three problems.

1) *Insufficient application*: The performance of many CNNs in landslide detection has not been exploited.
2) *Poor efficiency*: Landslides are a macroscopic geological hazard, and deeper deep networks will result in reduced efficiency.
3) *Scarce samples*: Landslide areas usually have complex background objects, and landslide samples are relatively scant compared with vegetation, water and rural areas.

To solve these problems, we choose dense convolutional networks for landslide detection. DenseNets alleviate the vanishing gradient problem, enhance feature transmission, support reusing features, and prominently decrease network parameters [45]. In landslide detection, a deeper DenseNet can not only exploit the potential of CNNs, but also reduce computational costs because of feature reuse and fewer parameters. Furthermore, DenseNet is not easy to overfit and has a strong generalization ability, which is suitable for fewer samples in landslide detection.

The purpose of this article is to explore the potential of the deep learning network DenseNet in landslide detection with only a small number of training samples to explore and try to solve the problems faced by deep learning in the application of landslide recognition. The two main contributions of this article are as follows: explore the performance of DenseNet in landslide detection, and introduce more environmental factors to improve the performance of deep learning in landslide recognition.

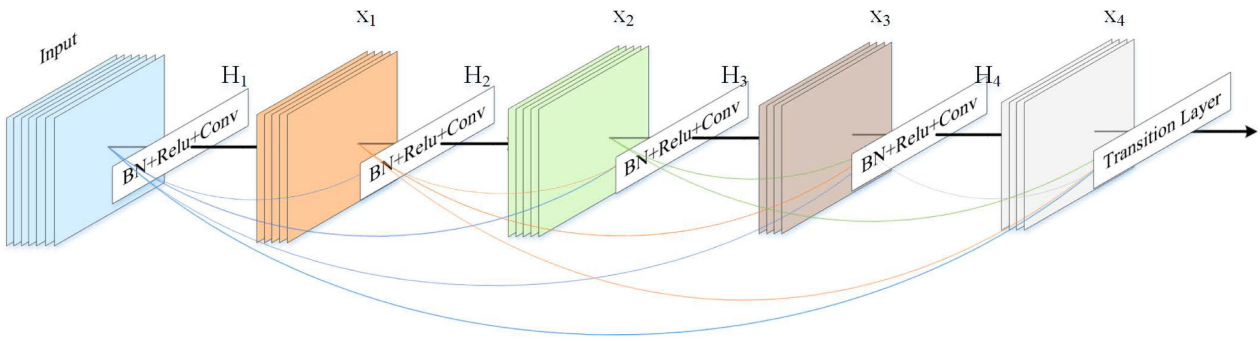

Fig. 1. Dense block.

II. Methods

A. DenseNet

Huang *et al.* proposed DenseNet at the conference on Computer Vision And Pattern Recognition in 2017 [45]. The design inspiration is the same as that of deep residual networks (ResNet) [46] and highway networks [47]. Although these types of networks are structurally different, their essence is to use shortcut connections from shallow layers to deep layers. This connection method can avoid the problem of gradient vanishing with the deepening of the network [48]. DenseNet adopts a more radical short connection mode: to maximize information flow between the layers in the network, they directly connect all layers (with matching feature map sizes) together [45]. Its dense connectivity is shown in Fig. 1.

In contrast to ResNet, DenseNet proposes a dense connectivity mechanism: it connects all the layers. Specifically, each layer will accept all previous feature layers, and then together as the next module input. It establishes dense connectivity between all the front layers and back layers, and its name comes from it. For the L-layer network, DenseNet includes a total of L ($L + 1$)/2 connections. Consequently, the layer receives the feature-maps of all preceding layers, as input

$$x_l = F_l([x_0, x_1, \ldots, x_{l-1}]) \tag{1}$$

where $[x_0, x_1, \ldots, x_{l-1}]$ refers to the concatenation of the feature-maps produced in layers $0, \ldots, l-1$. $F_l(\bullet)$represents a nonlinear conversion function. DenseNet inherits the advantages of ResNet, but the network parameters and calculations are greatly reduced, which is very meaningful for large-scale landslide detection tasks and can improve detection efficiency. In addition to fewer parameters, DenseNet also improves the flow of the entire network features and gradients [45]. The original input data and the gradient of the loss function can be passed to each layer, as if all layers are under deep supervision [49].

B. DenseNet-BC

CNN networks generally have to pass pooling or convolution with strides greater than 1 to reduce the feature map width and height, while the dense connectivity framework requires the feature map size to be consistent. To solve this problem, the structure of the dense block and transition is used in the DenseNet network. Among them, the dense block is a module that contains multiple convolutional layers with dense connection mode. All the feature layers inside the dense block have the same width and height. Fig. 2 shows the network structure of DenseNet, which contains three dense blocks in total, and each dense block is connected by a transition.

The feature maps with the same size inside the dense block are connected together by channel combination. $F_l(\bullet)$ is a nonlinear function combined by three operations, and the three module sequences are batch normalization [50], rectified linear unit [51] and 3 $\times$ 3 convolution (Conv). Each layer in the dense block outputs k feature maps after $F_l(\bullet)$, and k is called the growth rate in DenseNet, which is a hyperparameter. In general, using a small k can obtain better performance. Assuming that the number of channels in the feature map of the input layer is k_0, then the number of channels in the l^{th} layer is $k_0 + k(l-1)$. As the number of layers increases, although k is set small, the input of dense blocks will be very large, but this is caused by feature reuse. To solve the problem of excessive input in deep layers, the bottleneck layer can be used inside dense blocks to reduce the amount of calculation, and 1x1 Conv (see Fig. 3) is added to the original structure, which is called DenseNet-B. A 1x1 Conv obtains 4*k feature maps, and its function is to compress feature layers, thereby improving the calculation efficiency.

The transition layer includes a convolution layer with a kernel size of 1 $\times$ 1 and an average pooling layer with a stride of 2, which can serve as a compression model. If the feature layer output by the dense block is m, then the transition layer can pass through a compression parameter θ, where θ is the compression rate. Usually, the value of $\theta$is less than 1 to compress the number of channels of the feature map and reduce DenseNet parameters. Adding bottleneck and transition modules to DenseNet can further reduce the number of feature maps and network parameters. The improved network is called DenseNet-BC. Considering the purpose of the research and DenesNet, this article selected three dense blocks, each of which contains six layers of dense connectivity. The number of feature maps in each 3x3 convolutional layer is 12, and the drop rate is 0.2. The network diagram is shown in Fig. 4. Furthermore, according to the features of the landslide, DenseNet uses dilation convolution, the dilation rate of each dense block is 5, 2, and 1 in order from shallow to deep [52]. The modified method can increase the receptive field without increasing network parameters so that the convolution

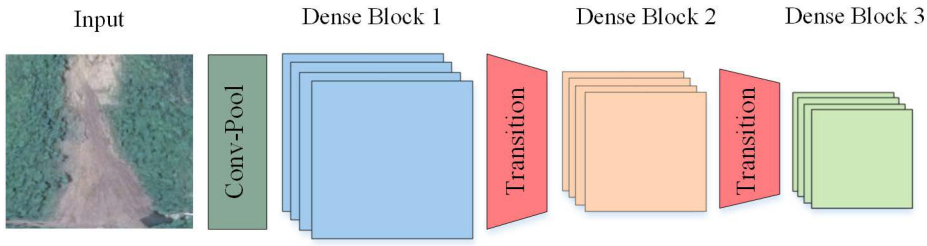

Fig. 2. DenseNet network using dense block + transition.

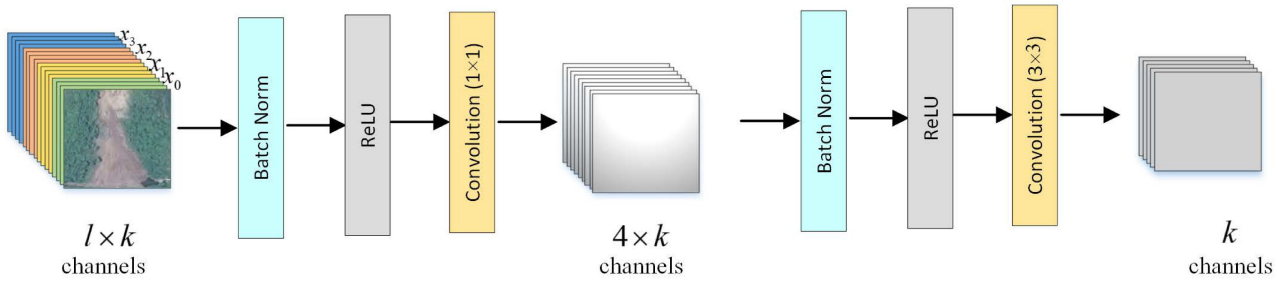

Fig. 3. DenseNet-B.

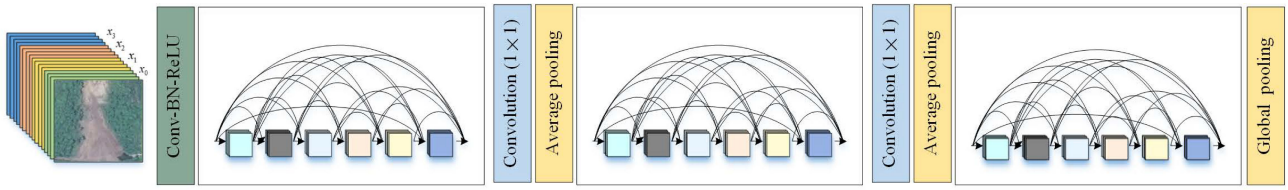

Fig. 4. DenseNet-BC.

can learn more complete semantic features of the landslide. The modified DenseNet has a total of 158 layers, but there are only 177 614 training parameters, which is much smaller than that of ResNet, VGG16 and other networks.

C. Landslide Sample Library

The occurrence and development of landslides are related to many factors, e.g., geology, geomorphology, land cover, and hydrological conditions [53]–[55]. According to the environment of the study area, aspect, slope, elevation, terrain relief, profile curvature, plan curvature, lithology, bedding structure, NDVI, MNDWI, distance to fault, and rivers are added to construct new landslide samples. These factors cannot only improve the accuracy of landslide detection but also identify potential landslides [56].

D. Flowchart of Landslide Detection

The entire experimental process consists of four parts. First, samples of landslide labels in the study area were prepared and the required factors were generated from geological maps, geographic information databases and remote sensing images. Second, the acquired factors were preprocessed and concatenated with the image, and then pixel patches were generated to divide the training and validation sets. Third, DenseNet and other models were used for landslide extraction. Finally, we evaluated and compared the performance of the landslide extraction model, and discussed the influence of some parameters on the experimental results. The complete experimental process adopted in this article is shown in Fig. 5.

E. Accuracy Evaluation

To evaluate the performance of DenseNet in landslide detection, precision, recall, F1 score [57], and kappa coefficients were used to quantitatively evaluate the model. In binary classification tasks, precision and recall are the two most common classification performance evaluation indicators. Precision, or positive sample accuracy rate, refers to the proportion of the predicted correct positive samples to the total predicted positive samples. Recall, also called sensitivity in some fields, refers to the ratio of the number of predicted positive samples to all true positive samples. The calculation formulas are

$$\text{precision} = \frac{\text{TP}}{\text{FP} + \text{TP}} \tag{2}$$

$$\text{recall} = \frac{\text{TP}}{\text{FN} + \text{TP}} \tag{3}$$

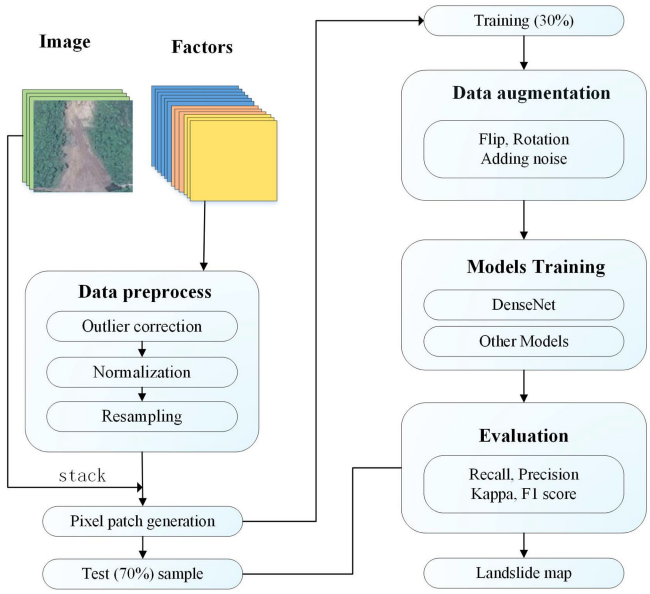

Fig. 5. Flowchart of landslide detection.

TABLE I
CONFUSION MATRIX DESCRIPTION IN OUR APPLICATION

True Value / Predicted Value	Landslides	Background
Landslides	True Positive (TP)	False Positive (FP)
Background	False Negative (FN)	True Negative (TN)

in which TP, FP, FN, and TN come from the confusion matrix (see Table I). TP refers to the number of positive samples that are correctly predicted, and TN refers to the number of is negative samples that are correctly predicted. FP is the number of negative samples predicted to be positive, and FN is the number of positive samples predicted to be negative.

Precision and recall are contradictory, so the F1 score is usually used to comprehensively evaluate the classification results. The F1 score is the harmonic average of precision and recall; a higher F1 score indicates better overall classification results. The formula is

$$F_1 = 2 \times \frac{\text{precision} \times \text{recall}}{\text{precision} + \text{recall}}. \tag{4}$$

The kappa coefficient is a method used to evaluate consistency in statistics, and we used it to appraise the accuracy of multiclassification models. Kappa can quantitatively appraise the consistency between the classification results and the true label. When its value is greater than 0.8, the consistency can be considered excellent. The Cohen kappa coefficient is defined and given by the following function:

$$\text{kappa} = \frac{p_0 - p_e}{1 - p_e} \tag{5}$$

$$p_e = \frac{(\text{TP} + \text{FN})(\text{TP} + \text{FP}) + (\text{FP} + \text{TN})(\text{TN} + \text{FN})}{n^2} \tag{6}$$

in which, p_0 is the overall accuracy, and n is the total samples.

TABLE II
SOURCE OF DIFFERENT APPLIED FACTORS

Data Type	Factors	Resolution/Scale	Source
Topography	Aspect	30m	GDEM
	Elevation	30m	GDEM
	Terrain relief	30m	GDEM
	Plan curvature	30m	GDEM
	Profile curvature	30m	GDEM
	Slope	30m	GDEM
Geology	Bedding structure	1:50000	Geological map
	Distance to fault	-	Geological map
	Lithology	1:50000	Geological map
Hydrology	Distance to rivers	-	GIS database
	MNDWI	30m	Landsat ETM+
Land cover	NDVI	30m	Landsat ETM+

III. EXPERIMENT

A. Study Area

The study site is in Hubei Province, including Zigui County and Badong County, in western Xiling Gorge (see Fig. 6). Its geographic range is approximately 110.30°E and 110.87°E, 30.02°N and 30.93°N, covering an area of approximately 396 km^2. The Yangtze River passes through the study area in a WNW-ESE direction. The area has a typical subtropical monsoon climate and is characterized by hot summers and cold winters. The rainy season is mainly concentrated from June to September, the precipitation can be as high as 200–300 mm per month, and the annual average rainfall is 1100 mm [57]. There are a total of 202 landslides in the study area, mainly distributed along the Yangtze River and its tributaries, covering an area of approximately 23.40 km 2. Larger landslides include Fanjiaping landslide, Kaziwan landslide, Huangtupo landslide, etc., accounting for 75% of the total landslide area. Landslides and collapses in the study area have caused many disasters to local people in history.

B. Data

The data include landslide label, high-resolution satellite imagery, and the study area environmental conditions described in Section II-C. The landslide label was constructed by using historical landslide record, interpretations of satellite images and field survey data which provided by the Headquarters for the prevention and control of geo-hazards in the Three Gorges Reservoir area. The high-resolution image comes from the ZY-3 satellite, 4 bands, with a resolution of 5.8 m, acquired in April 2013. These factors used in the experiments can be divided into four categories, and their sources are given in Table II.

After preprocessing these factors, they are superimposed with the remote sensing image to obtain a data cube of size $m \times n \times c$, where m and n are the width and height, respectively, and c is the number of channels. The main preprocessing operations are outlier correction, normalization, and resampling. This article is based on pixel-based landslide detection, using pixels as samples in the study area. Training samples and test samples are randomly selected in total samples. To verify the performance of the proposed method with only a small number of landslide

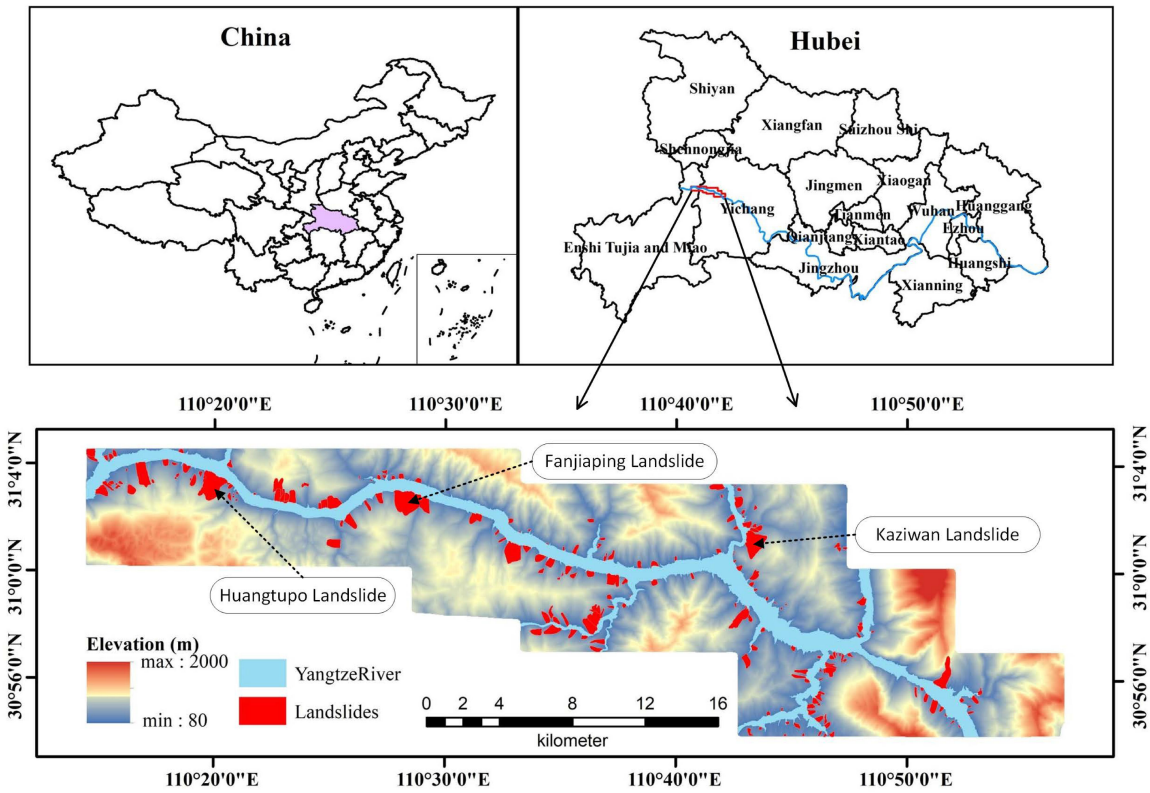

Fig. 6. Location of the study area.

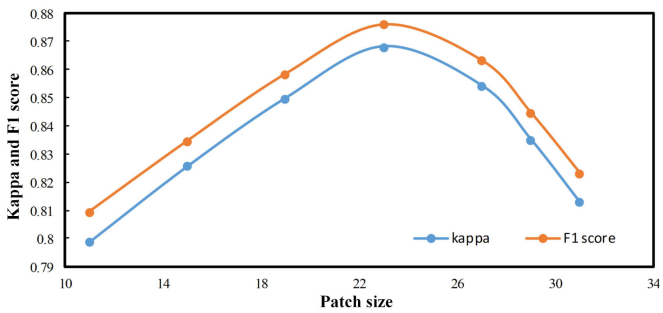

Fig. 7. Kappa and F1 score of different patch sizes.

samples, 30% of the existing samples are selected as training data, and the rest are test samples. The total number of dataset samples is 487 474, with the training sample of 146 242, and the test sample of 341 232. After data augmentation processing, the number of training samples is 584 968, and the number of test samples remains unchanged. The input of the model is a patch centered on the pixel [58], but the patch size affects the ability of the convolution kernel to learn features [59]. The experiment used the baseline DenseNet to select the optimal patch size. Seven different patch sizes were selected, and the F1 score and kappa were used as the evaluation indexes. Fig. 7 demonstrates the values of the kappa coefficient and F1 score under different patch sizes. When the path size was 23 × 23, the evaluation value reached the highest value. Therefore, in all comparative experiments, a patch size of 23 × 23 was used. Because landslides have rotation and translation invariance, and landslide samples are generally difficult to obtain, the training samples are data augmented. The purpose of data augmentation is to ensure that the model can still learn the general characteristics of landslides with only a few training samples. The augmentation methods are horizontal flipping, adding Gaussian noise, and rotation.

C. Experimental Configuration

The experimental environment of the article is a personal computer equipped with an Intel Core i3-8100 processor, 8 GB memory, and Nvidia GeForce GTX 1060 graphics card. All source code is programmed using the Python language under the deep learning framework TensorFlow. According to the research purpose, comparative experiments were designed: three different input datasets on DenseNet and three traditional CNN networks compared with DenseNet.; DenseNet with SVM, and RF.

IV. Results and Analysis

A. Performance Analysis of Training Sample Type

To verify that the added surface topographical factors improve the performance of landslide detection, three different data types are entered into the DenseNet model for landslide detection. The results are shown in Fig. 8.

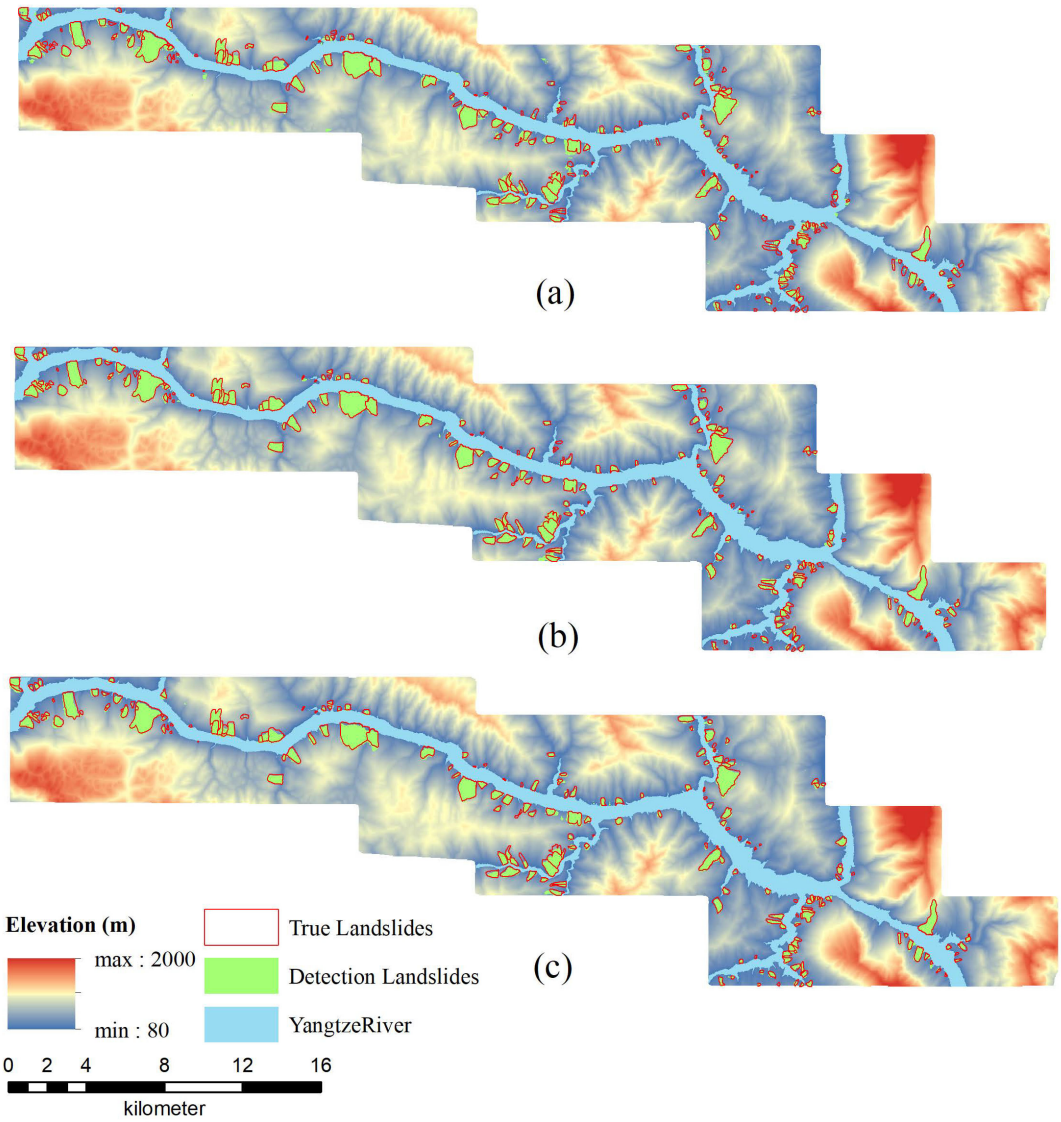

Fig. 8. Three kinds of training sample detection results. (a) RS image. (b) Factors. (c) RS image + factor.

Fig. 8(a) demonstrates the result of remote sensing image detection. It can be observed from the result that the error and missed cases are obvious, and the results are not satisfactory. Overall, most of the identified landslides do not match the actual landslide boundaries, and there are phenomena beyond the boundaries, or only a part of the landslides is identified. Most small landslides are completely unrecognizable or only a small number of landslide pixels were recognized. Some landslide bodies that are close to each other cannot accurately distinguish the boundary. There are two reasons for this phenomenon. The first is that the different categories samples in the study area are severely unbalanced. Statistics show that the ratio of nonlandslide pixels to landslide pixels is 15:1. Another reason is the training data. Some small landslides are affected by imaging technology or vegetation coverage, which cannot be identified by optical images alone. Fig. 8(b) demonstrates the result of factor detection. It can be observed that the overall landslide map is satisfactory, the number of completely unrecognized landslides is reduced, and most of the landslide areas are consistent with the actual boundary. Fig. 8(c) is the result of using factor + image detection. The overall detection result is not much different from using a factor. The detection results show that the causative factors play an important role in landslide detection, and the new landslide sample library is effective.

To quantitatively evaluate the model performance and landslide detection results of three different training samples, the confusion matrix is used to calculate the four evaluation factors mentioned in Section II-E, and the evaluation indexes are shown in Table III. Image + factors exhibit the highest precision, F1, and kappa coefficients, but the recall value is lower than the factors. The higher the recall is, the more landslides are recognized, and the higher the precision is, the more landslides are correctly identified. The number of landslides identified by factors is high, but the precision is low. A comprehensive evaluation, image + factor training sample detection is the best. The qualitative and quantitative appraisal of the results of the three different training

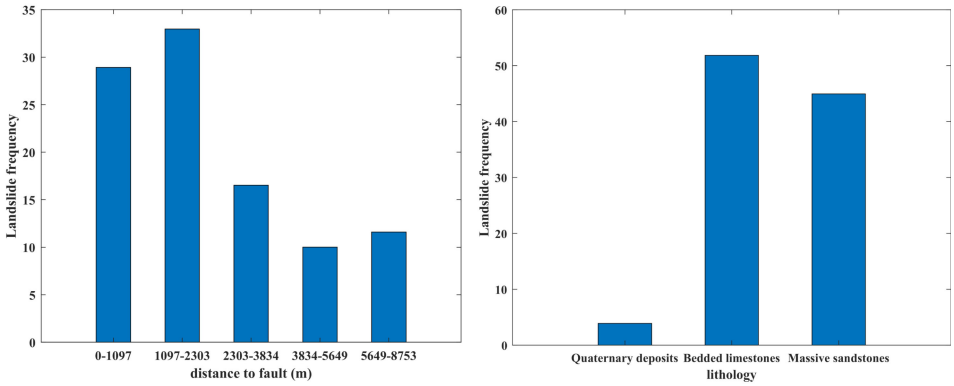

Fig. 9 Landslide frequency in factors intervals.

TABLE III
PERFORMANCE VALUE OF DIFFERENT TRAINING SAMPLE

	Recall/%	Precision/%	F1	Kappa
RS image	80.62	77.08	0.7880	0.7745
factor	**89.60**	85.69	0.8760	0.8681
RS Image+ factor	86.76	**89.07**	**0.8790**	**0.8715**

TABLE IV
PERFORMANCE VALUE OF DIFFERENT

	Recall/%	Precision/%	F1	Kappa
1D-CNN	25.45	59.05	0.3557	0.3320
2D-CNN	80.01	83.93	0.8192	0.8082
SS-CNN	81.15	**91.33**	0.8594	0.8512
DenseNet	**86.76**	89.07	**0.8790**	**0.8715**

data types shows that the landslide factors provide additional information and improve the accuracy of landslide detection, and these factors are equivalent to increasing the attribute features of the landslide. Taking the topography factor as an example, landslides are controlled by factors such as elevation, slope, and aspect. As shown in Fig. 9, the distribution of landslides in different intervals of the distance to fault and lithology is distinguishable. As long as the distribution is different, CNN can use this difference to learn the characteristics of the landslide to distinguish it from the background and help improve the performance of the model.

B. Performance Analysis of Different CNN Model

To illustrate the performance of the DenseNet for landslide detection, three traditional CNNs are compared: 1-D-CNN [60], 2-D-CNN [61] and spatial-spectral CNN (SS-CNN) [62]. All the experimental hyperparameters, training data, and other variables are consistent. 2-D-CNN can extract the spatial features of landslides, 1-D-CNN can extract the "spectral" features of landslide pixels at each factor layer, and SS-CNN combines these two features. The results are shown as follows.

Fig. 10(a) demonstrates the result map of the 1-D-CNN model. It can be seen in the figure that many landslides cannot be identified. Even though identified landslide area is seriously inconsistent with the actual range, the noise phenomenon of the landslide map is serious. Fig. 10(b) shows the result of the 2-D-CNN model. Compared with the 1-D-CNN detection results, the ability of landslide detection is significantly improved which only has a small unrecognized area inside the landslide, and the noise phenomenon is significantly reduced. Fig. 10(c) shows the result of the SS-CNN model. Due to the combination of spatial and factor features, almost all landslide areas can be well identified, and a small number of small landslides cannot be identified. The landslide graph is smooth and the noise phenomenon is significantly reduced. The boundary of the landslide is closer to the actual landslide ranges. Fig. 10(d) shows the results of the DenseNet model. The detection result is closest to the actual landslide range, the landslide map is noise-free and the boundaries almost completely match.

The quantitative evaluation of these four models is given in Table IV. The DenseNet model has a precision of 89.07%, a recall of 86.76%, an F1 of 0.8790, and a kappa of 0.8715. In addition to precision, other evaluation index values of DenseNet are the highest. A comparison of the 2-D-CNN and 1-D-CNN shows that the spatial characteristics of landslides are the most important identification signs. Comparing SS-CNN and 2-D-CNN, it shows that the fusion of different types of landslide features can also play a positive role. Comparing DenseNet and SS-CNN shows that multilevel feature fusion is better than using only the last feature layer. Although DenseNet has a higher rate of misrecognition of landslides, more landslides can be identified and the overall effect is the best. Furthermore, Fig. 11 shows the convergence curves; we find that for the same number of iterations, training loss and validation loss of DenseNet are lower than other models, which means that we can obtain satisfactory results with fewer iterations. Thus, it can save time and improve efficiency in large-scale landslide detection applications. 1-D-CNN, 2-D-CNN, and SS-CNN are three typical CNN feature extraction methods. Most of the CNN models used for landslide recognition are 2-D-CNN and use high-resolution images, so they have achieved good results. However, in large-scale landslide recognition scenes, medium-resolution images are more suitable. This part of the experiment explores the performance of these three models in landslide

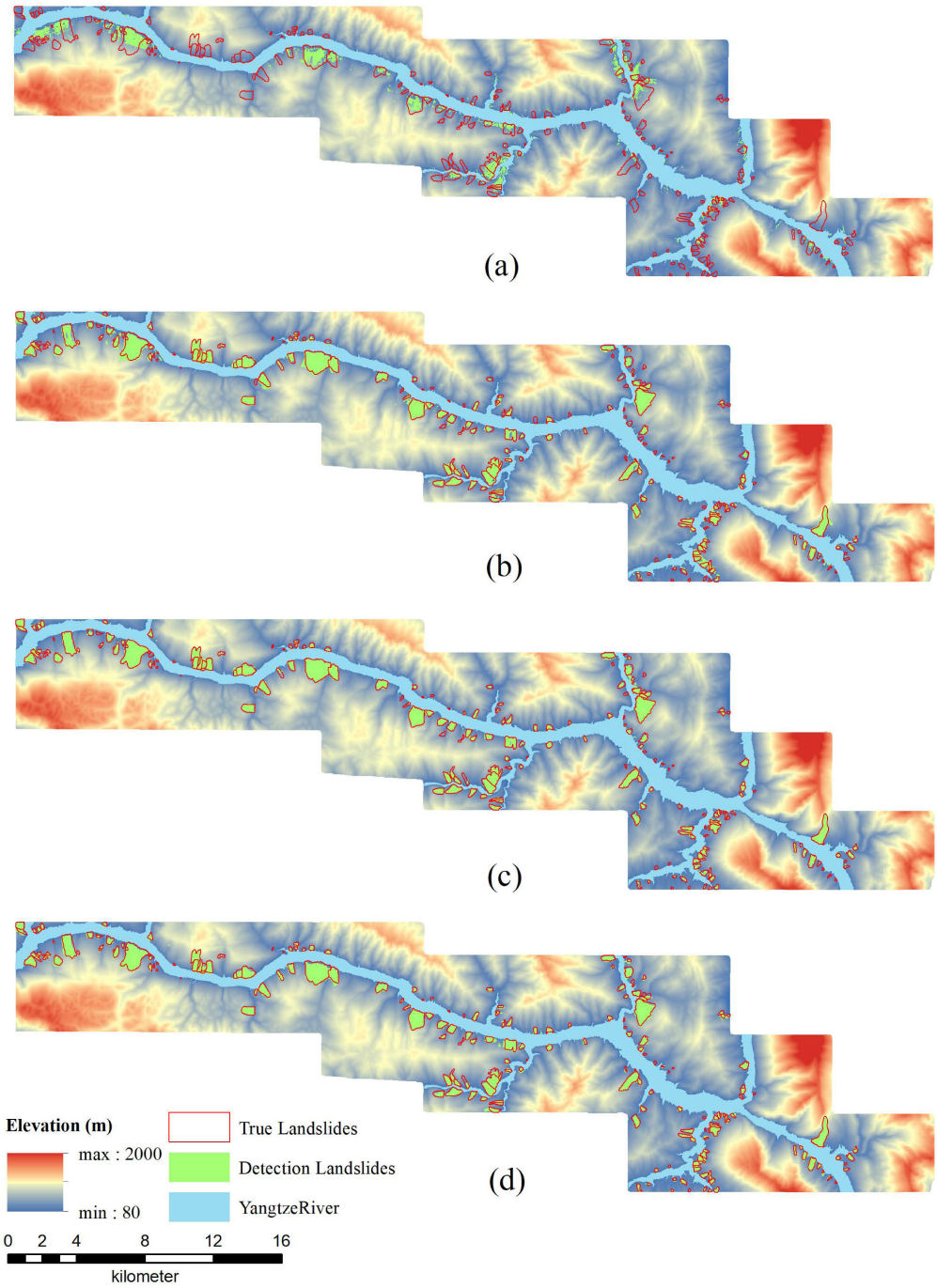

Fig. 10. Four model detection results. (a) 1-D-CNN, (b) 2-D-CNN. (c) SS-CNN. (d) DenseNet.

recognition, and the proposed method can balance efficiency and accuracy in landslide recognition in extensive areas.

C. DenseNet Optimization Analysis

Landslide samples are difficult to obtain in practice, but deep learning model training requires a large number of training samples. Therefore, in the training phase, data augmentation techniques are adopted. Data augmentation technology can improve model generalization ability and robustness. Fine-tuning technology can solve bad cases in the recognition results well. This part of the experiment explores data augmentation and fine-tuning, and the detection maps are shown in Fig. 12.

In Fig. 12, the landslide map after fine-tuning and data augment is comprehensive and smooth, and its quantitative evaluation is given in Table V. The DenseNet model has a precision of 95.17%, a recall of 94.92%, and F1 of 0.9505, and a kappa of 0.9474, F1, and kappa are nearly 7% higher than baseline DenseNet. Experimental results show that through data augmentation and fine-tuning, the overall effect of landslide

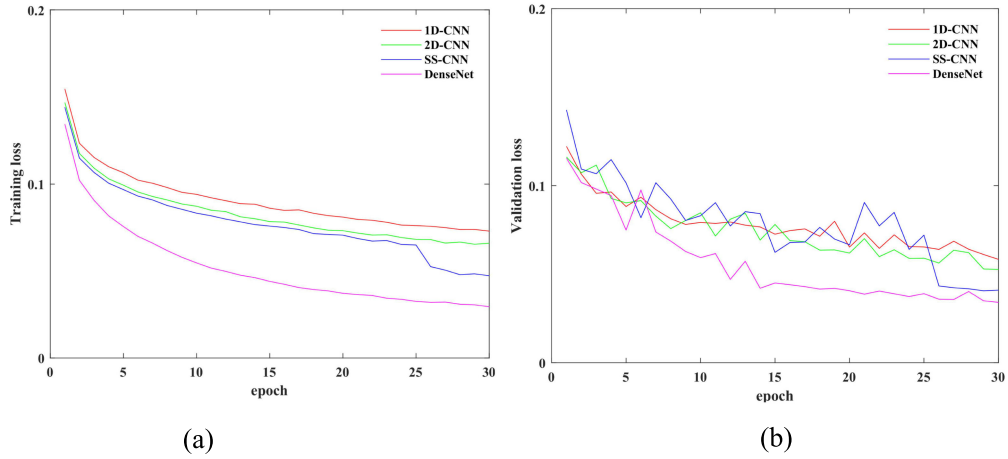

Fig. 11. Convergence curves of three CNN models. (a) Training samples. (b) Validation samples.

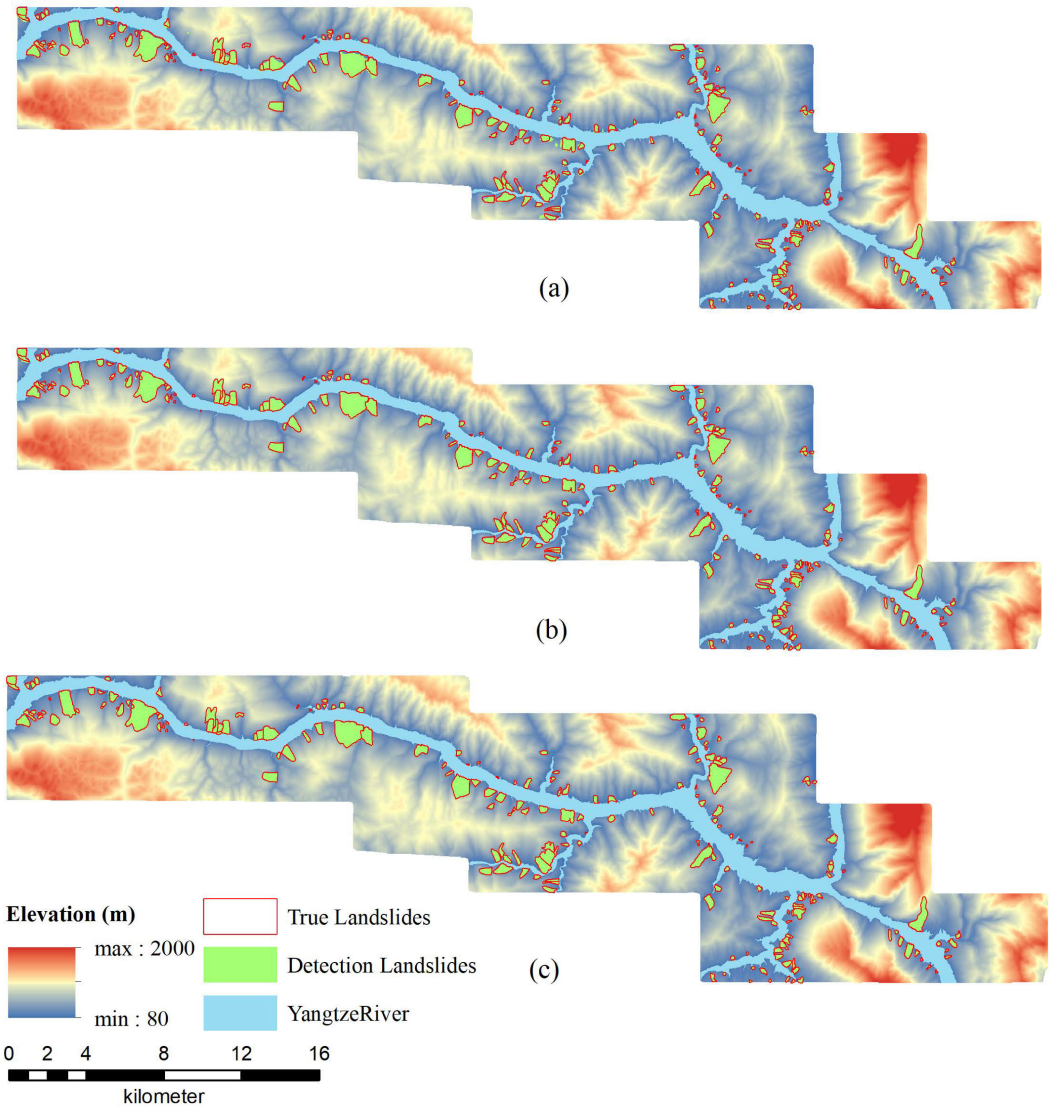

Fig. 12. DenseNet optimization results. (a) Baseline DenseNet. (b) DenseNet with data augment. (c) DenseNet with data augment and fine-tuning.

TABLE V
PERFORMANCE VALUE OF OPTIMIZATION STRATEGY

	Recall/%	Precision/%	F1	Kappa
Baseline	86.76	89.07	0.8790	0.8715
Data augment	92.22	94.47	0.9333	0.9292
Fine-tuning	**94.92**	**95.17**	**0.9505**	**0.9474**

TABLE VI
PERFORMANCE VALUE OF DENSENET WITH TRADITIONAL METHODS

	F1	Kappa
SVM	0.7039	0.6895
RF	0.4524	0.4349
DenseNet	**0.9505**	**0.9474**

recognition can be further improved. Data augmentation enables the model to learn the general characteristics of the landslide, and the introduction of noise makes the model more suitable for complex landslide areas, and has the greatest impact on the improvement of the model.

D. Comparison With Traditional Methods

Furthermore, we compare the landslide detection performance of DenseNet and SVM [63], and RF [39]. The SVM penalty parameter is 1.0, and the kernel function is the radial basis function. The RF has 10 decision trees and the maximum depth is 50. All the experiments only use 30% of the samples as training data, and the quantitative evaluation results are shown in Table VI.

It can be seen in the evaluation results that when only a small number (30%) of the samples are used, the performance of SVM and RF is poor, and the kappa coefficients are only 0.6895 and 0.4349, respectively, while the kappa coefficient of DenseNet is 0.9474. Comparing DenseNet with traditional ML algorithms, when there are scarce samples in practical applications, the performance of ML will be very poor, but the improved DenseNet is not be affected. Obviously, our proposed method is suitable for large-scale landslide recognition scenarios that lack samples.

V. DISCUSSION

To verify the influence of various environmental factors on the detection performance of the model, we analyzed the importance of 12 factors on the landslide before modeling. In this article, the information gain ratio (IGR) was used to analyze the training set [64]. The higher the IGR value was, the greater the influence of this factor on the occurrence of landslides. A factor with an IGR value of 0 means that it does not contribute to the occurrence of the landslide and should be eliminated.

As shown in Fig. 13, the IGR values of all 12 factors were greater than 0, indicating that these factors contribute to our landslide detection model in the study area. Among these factors, distance to rivers had the most significant impact on landslides, because the landslides in the study area are reservoir slope landslides. Next are the aspect, slope, elevation, and other topographic and geomorphic factors.

In addition, based on different types of factors, 6 sets of comparative experiments were performed to verify the role of

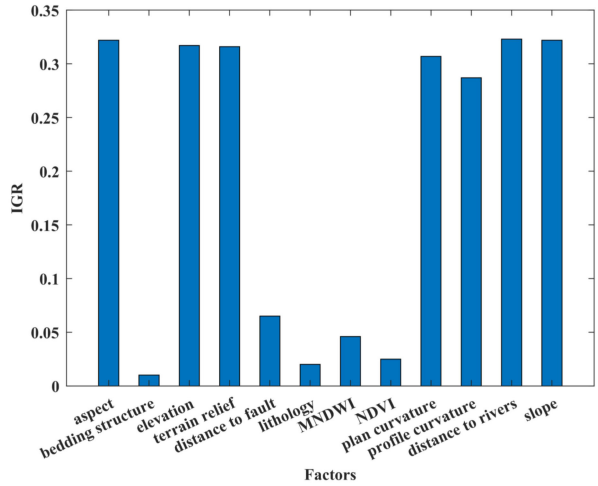

Fig. 13. IGR of the environmental factors.

TABLE VII
PERFORMANC OF DIFFERENT FACTORS TYPE

	F1	Kappa
All factors	**0.8760**	**0.8681**
Topography	0.8209	0.8104
Geology	0.7846	0.7721
HL	0.6881	0.6722
Topography + Geology	0.8674	0.8594
Topography + HL	0.8302	0.8204
Geology + HL	0.8085	0.7975

the factors in the landslide detection model. For convenience, the hydrology and land cover factors are grouped into one category, denoted as HL.

As given in Table VII, the DenseNet model that used all factors had the best landslide detection performance. Among them, topographic factors played the most important role, followed by geology and HL factors. If any factor was reduced, the performance of the model decreased. Overall, all selected landslide environmental factors were used to model landslide detection. Although studies have shown that some factors have a negative effect on model recognition [65], in this article, all types of factors had a positive effect on the detection model. The choice of factors was affected by the environment of the study area, the type of landslide and the method adopted. Therefore, when modeling, decide which factors to choose according to your own conditions.

VI. CONCLUSION AND FUTURE LINES

In this article, a novel landslide sample library was established by adding environmental factors. Based on these landslide sample libraries, the DenseNet architecture was used to detect and map the existing and historical landslides in the Three Gorges area of China. Experimental results show that the proposed method can accurately identify landslides in a large area with fewer training samples, which is beyond ordinary CNN and traditional ML methods. Furthermore, the proposed method has few model parameters, and a faster convergence speed than the general deep CNN, so it has promise applicability in

large area landslide recognition scenarios lacking samples. The poor recognition ability of this method on microlandslides is a problem to be solved in the future.

REFERENCES

[1] M. Scaioni, L. Laura M. Valentina, and M.Papini, "Remote sensing for landslide investigations: An overview of recent achievements and perspectives," *Remote Sens.,* vol. 6, no. 10, pp. 9600–9652, Oct. 2014.

[2] Z. Chen, X. Meng Y. Yin, T. Dijkstra, M. Winter, and J. Wasowski, "Landslide research in China," *Quart. J. Eng. Geol. Hydrogeol.*, vol. 49, no. 4, pp. 279–285, Nov. 2016.

[3] H. Keqiang, L. Xiangran, Y. Xueqing, and G. Dong, "The landslides in the three Gorges reservoir region, China and the effects of water storage and rain on their stability," *Environ. Geol.,* vol. 55, no. 1, pp. 55–63, Jul. 2008.

[4] B. Huang, S. C. Wang, and Y. B. Zhao, "Impulse waves in reservoirs generated by landslides into shallow water," *Coastal Eng.,* vol. 123, pp. 52–61, May. 2017.

[5] N. Prakash, A. Manconi, and S. Loew, "Mapping landslides on EO data: Performance of deep learning models vs. traditional machine learning models," *Remote Sens.,* vol. 12, no. 3, pp. 346, Jan. 2020.

[6] M. Mezaal, P. Biswajeet, and R. Hossein, " Improving landslide detection from airborne laser scanning data using optimized Dempster-Shafer," *Remote Sens.,* vol. 10, no. 7, pp. 1029, Jun. 2018.

[7] F. Guzzetti *et al.*, "Landslide inventory maps: New tools for an old problem," *Earth-Sci. Rev.,* vol. 112, no. 1–2, pp. 42–66, Apr. 2012.

[8] S. M. Arbanas and Ž. Arbanas, "Landslide mapping and monitoring: Review of conventional and advanced techniques," in *Proc. 4th Symp. Macedonian Assoc. Geotech.,* 2014, pp. 57–22.

[9] A. G. Xing *et al.*, "Dynamic analysis and field investigation of a fluidized landslide in Guanling, Guizhou, China," *Eng. Geol.,* vol. 181, pp. 1–14, Oct. 2014.

[10] P. V. Gorsevski, M. K. Brown K. Panter, C. M. Onasch, A. Simic, and J. Snyder, "Landslide detection and susceptibility mapping using LiDAR and an artificial neural network approach: A case study in the Cuyahoga valley national park, Ohio," *Landslides,* vol. 13, no. 3, pp. 467–484, Jun. 2016.

[11] M. Zhu, Y. He, and Q. He, "A review of researches on deep learning in remote sensing application," *Int. J. Geosci.,* vol. 10, no. 1, pp. 1–11, 2019.

[12] D. Li, Q. Tong, R. Li, J. Y. Gong, and L. P. Zhang, "Current issues in high-resolution earth observation technology," *Sci. China Earth Sci.,* vol. 55, no. 7, pp. 1043–1051, Jul. 2012.

[13] P. Liu *et al.*, "Using advanced InSAR time series techniques to monitor landslide movements in badong of the three Gorges region, China," *Int. J. Appl. Earth Observ. Geoinf.,* vol. 21, pp. 253–264, Apr. 2013.

[14] G. Qiao *et al.*, "Landslide investigation with remote sensing and sensor network: From susceptibility mapping and Scaled-down simulation towards in situ sensor network design," *Remote Sens.,* vol. 5, no. 9, pp. 4319–4346, Sep. 2013.

[15] S. Sarkar and D. P. Kanungo, "An integrated approach for landslide susceptibility mapping using remote sensing and GIS," *Photogramm. Eng. Remote Sens.,* vol. 70, no. 70, pp. 617–626, 2015.

[16] B. Adia, S. P. D. Alfonso, and M. Danaeetal, "Collect earth: Land use and land cover assessment through augmented visual interpretation," *Remote Sens.,* vol. 8, no. 10, pp. 1–24, 2016.

[17] H. Gao, J. Liu, A. E. Eneji, L. Han, and L. Tan, "Using modified remote sensing imagery to interpret changes in cultivated land under saline-alkali conditions," *Sustainability,* vol. 8, no. 7, pp. 619–632, Jul. 2016.

[18] T. R. Martha, N. Kerle, C. J. V. Westen, V. Jetten, and K.V. Kumar, "Object-oriented analysis of multi-temporal panchromatic images for creation of historical landslide inventories," *ISPRS-J. Photogramm. Remote Sens.,* vol. 67, pp. 105–119, Jan. 2012.

[19] S. Bai *et al.*, "GIS-based logistic regression for landslide susceptibility mapping of the Zhongxian segment in the three Gorges area, China," *Geomorphology,* vol. 115, no. 1/2, pp. 23–31, Feb. 2010.

[20] S. L. Das *et al.*, "Image processing methods for computer-aided interpretation of cell lines for cancer studies," *Biomed. Res.,* vol. 28, no. 10, pp. 4294–4298, 2017.

[21] T. Kavzoglu, I. Colkesen, and E. K. Sahin, "Machine learning techniques in landslide susceptibility mapping: A survey and a case study," in *Landslides: Theory, Practice and Modelling. Advances in Natural and Technological Hazards Research*, vol. 50, S. Pradhan, V. Vishal, and T. Singh Eds., New York, NY, USA: Springer, 2019.

[22] M. Marjanovi *et al.*, "Landslide assessment of the stara basin (Croatia) using machine learning algorithms," *Acta Geotechnica Slovenica,* vol. 8, no. 2, pp. 45–55, 2011.

[23] D. Costanzo, "Factors selection in landslide susceptibility modelling on large scale following the GIS matrix method: Application to the river Beiro basin (Spain)," *Nat. Hazards Earth Syst Sci.,* vol. 12, no. 2, pp. 327–340, Feb. 2012.

[24] J. N. Goetz *et al.*, "Evaluating machine learning and statistical prediction techniques for landslide susceptibility modeling," *Comput. Geosci.,* vol. 81, pp. 1–11, Aug. 2015.

[25] B. T. Pham *et al.*, "Rotation forest fuzzy rule-based classifier ensemble for spatial prediction of landslides using GIS," *Nat. Hazards,* vol. 83, pp. 97–127, Aug. 2016.

[26] A. Brenning, "Spatial prediction models for landslide hazards: Review, comparison and evaluation," *Nat. Hazard Earth Syst.,* vol. 5, no. 6, pp. 853–862, 2005.

[27] E. Pagot and M. Pesaresi, "Systematic study of the urban post conflict change classification performance using spectral and structural features in a support vector machine," *IEEE J. Sel. Topics Appl. Earth Observ. Remote Sens.,* vol. 1, no. 2, pp. 120–128, Jun. 2008.

[28] F. Fiorucci *et al.*, "Seasonal landslide mapping and estimation of landslide mobilization rates using aerial and satellite images," *Geomorphology,* vol. 129, no. 1/2, pp. 59–70, Jun. 2011.

[29] M. Constantin *et al.*, "Landslide susceptibility assessment using the bivariate statistical analysis and the index of entropy in the Sibiciu basin (Romania)," *Environ. Earth Sci.,* vol. 63, no. 2, pp. 397–406, May. 2011.

[30] E. Maggiori, Y. Tarabalka, G. Charpiat, and P. Alliez, "Convolutional neural networks for large-scale remote-sensing image classification," *IEEE Trans. Geosci. Remote Sens.,* vol. 55, no. 2, pp. 645–657, Feb. 2017.

[31] M. A. Kolodny, R. Mccoppin, and M. Rizki, "Deep learning for image classification," in *Proc. SPIE Int. Soc. Opt. Eng.*, 2014, p. 90790T.1-10.

[32] S. Ren, K. He, R. Girshick, and J. Sun, "Faster R-CNN: Towards real-time object detection with region proposal networks," *IEEE Trans. Pattern Anal. Mach. Intell.,* vol. 39, no. 6, pp. 1137–1149, Jun. 2017.

[33] Y. Tian *et al.*, "Metal object detection for electric vehicle inductive power transfer systems based on hyperspectral imaging," *Measurement,* vol. 168, Jan. 2021, Art. no. 108493.

[34] F. Richardson, D. Reynolds, and N. Dehak, "Deep neural network approaches to speaker and language recognition," *IEEE Signal Process. Lett.,* vol. 22, no. 10, pp. 1671–1675, Oct. 2015.

[35] W. Sai, X. Suning P. Ling, Z. Wang, and N. Wang, "A rapid extraction of landslide disaster information research based on GF-1 image," *Proc. SPIE, Int. Soc. Opt. Eng.,* vol. 9669, no. 1, pp. 307–314, 2015.

[36] R. N. Keyport, T. Oommen T. R. Martha, K.S. Sajinkumarac, and J. S.Gierkea, "A comparative analysis of pixel- and object-based detection of landslides from very high-resolution images," *Int. J. Appl. Earth Observ. Geoinf.,* vol. 64, pp. 1–11, Feb. 2018.

[37] H. Lu *et al.*, "Landslides information extraction using object-oriented image analysis paradigm based on deep learning and transfer learning," *Remote Sens.,* vol. 12, no. 5, p. 752 Feb. 2020.

[38] Y. Lecun, Y. Bengio, and G. Hinton, "Deep learning," *Nature,* vol. 521, no. 7553, pp. 436–444, May. 2015.

[39] O. Ghorbanzadeh, T. Blaschke, K. Gholamnia, S. R. Meena, D. Tiede, and J. Aryal, "Evaluation of different machine learning methods and deep-learning convolutional neural networks for landslide detection," *Remote Sens.,* vol. 11, no. 2, p. 196, 2019.

[40] S. R. Meena *et al.*, "Rapid mapping of landslides in the western ghats (India) triggered by 2018 extreme monsoon rainfall using a deep learning approach," *Landslides*, vol. 18, pp. 1937–1950 , 2021.

[41] Y. Yi and W. Zhang, "A new deep-learning-based approach for earthquake-triggered landslide detection from single-temporal Rapideye satellite imagery," *IEEE J. Sel. Topics Appl. Earth Observ. Remote Sens.*, vol. 13, pp. 6166–6176, Oct. 2020.

[42] W. Shi, M. Zhang, H. Ke, X. Fang, Z. Zhan, and S. Chen, "Landslide recognition by deep convolutional neural network and change detection," *IEEE Trans. Geosci. Remote Sens*, vol. 59, no.6, pp. 4654–4672, Jun. 2021.

[43] M. I. Sameen and B. Pradhan, "Landslide detection using residual networks and the fusion of spectral and topographic information," *IEEE Access,* vol. 7, pp. 114363–114373, 2019.

[44] B. Yu, F. Chen, and C. Xu, "Landslide detection based on contour-based deep learning framework in case of national scale of Nepal in 2015," *Comput. Geosci.,* vol. 135, pp. 104388, Feb. 2020.

[45] H. Gao *et al.*, "Densely connected convolutional networks," in *Proc. Comput. Vis. Pattern Recognit.*, 2017, pp. 2261–2269.

[46] K. He, X. Zhang, S. Ren, and J. Sun, "Deep residual learning for image recognition," in *Proc. Comput. Vis. Pattern Recognit.*, 2016, pp. 770–778.

[47] R. K. Srivastava, K. Greff, and J. Schmidhuber, "Training very deep networks," in *Proc. Adv. Neural Inf. Proces. Syst.*, 2015, pp. 2377–2385.

[48] K. He and J. Sun, "Convolutional neural networks at constrained time cost," in *Proc. Comput. Vis. Pattern Recognit.*, 2015, pp. 5353–5360.

[49] C. Y. Lee, S. Xie, P. Gallagher, Z. Zhang, and Z. Tu, "Deeply-supervised nets," *J. Mach. Learn. Res.,* vol. 38, pp. 562–570, 2015.

[50] S. Wu *et al.*, "*L*1-Norm batch normalization for efficient training of deep neural networks," *IEEE Trans. Neural Netw. Learn. Syst.,* vol. 30, no. 7, pp. 2043–2051, Jul. 2019.

[51] V. Nair and G. E. Hinton, "Rectified linear units improve restricted Boltzmann machines," in *Proc. Int. Conf. Mach. Learn.*,2010, pp. 807–814.

[52] X. Lei, H. Pan, and X. Huang, "A dilated CNN model for image classification," *IEEE Access,* vol. 7, pp. 124087–124095, 2019.

[53] B. Pradhan and S. Lee, "Landslide susceptibility assessment and factor effect analysis: Backpropagation artificial neural networks and their comparison with frequency ratio and bivariate logistic regression modelling," *Environ. Model. Soft.,* vol. 25, no. 6, pp. 747–759, Jun. 2010.

[54] T. Kavzoglu, E. Kutlug Sahin, and I. Colkesen, "Selecting optimal conditioning factors in shallow translational landslide susceptibility mapping using genetic algorithm," *Eng. Geol.,* vol. 192, pp. 101–112, Jun. 2015.

[55] W. Chen, H. R. Pourghasemi, and S. A. Naghibi, "Prioritization of landslide conditioning factors and its spatial modeling in Shangnan county, china using GIS-based data mining algorithms," *Bull. Eng. Geol. Environ.*, vol. 77, no. 2, pp. 611–629, May. 2018.

[56] J. S. Kargel *et al.*, "Geomorphic and geologic controls of geohazards induced by Nepals 2015 Gorkha," *Science,* vol. 351, no. 6269, p. aac8353, Jan. 2016.

[57] T. Chen, R. Niu, and X. Jia, "A comparison of information value and logistic regression models in landslide susceptibility mapping by using GIS," *Environ. Earth Sci.,* vol. 75, no. 10, p. 867, 2016.

[58] O. Ghorbanzadeh and T. Blaschke, "Optimizing sample patches selection of CNN to improve the MIoU on landslide detection," in *Proc. Int. Conf. Geograph. Inf. Syst. Theory, Appl. Manag.*, 2019, pp. 33–40.

[59] Y. Yi *et al.*, "Landslide susceptibility mapping using multiscale sampling strategy and convolutional neural network: A case study in Jiuzhaigou region," *Catena,* vol. 195, Dec 2020, Art. no. 104851.

[60] L. Dong, F. Wei, M. Zhou, and K. Xu, "Question answering over freebase with multi-column convolutional neural networks," in *Proc. Conf. Annu. Meeting Assoc. Comput. Linguistics Int. Joint Conf. Nat. Lang. Process.*, 2015, pp. 260–269.

[61] X. Xu, W. Li, Q. Ran, Q. Du, L. Gao, and B. Zhang, "Multisource remote sensing data classification based on convolutional neural network," *IEEE Trans. Geosci. Remote Sens.,* vol. 56, no. 2, pp. 937–949, Feb. 2018.

[62] S. Mei, J. Ji, J. Hou, X. Li, and Q. Du, "Learning sensor-specific spatial-spectral features of hyperspectral images via convolutional neural networks," *IEEE Trans. Geosci. Remote Sens.,* vol. 55, no. 8, pp. 4520–4533, Aug. 2017.

[63] D. T. Bui, A. T. Tran, H. Klempe, B. Pradhan, and I. Revhaug, "Spatial prediction models for shallow landslide hazards: A comparative assessment of the efficacy of support vector machines, artificial neural networks, kernel logistic regression, and logistic model tree," *Landslides,* vol. 13, no. 2, pp. 361–378, Apr. 2016.

[64] Y. Wang, Z. Fang, and H. Hong, "Comparison of convolutional neural networks for landslide susceptibility mapping in Yanshan county, China," *Sci. Total Envion.,* vol. 666, pp. 975–993, May. 2019.

[65] O. Ghorbanzadeh, S. R. Meena, H. Shahabi, S. T. Piralilou, and Z. Lv, "Landslide mapping using two main deep-learning convolution neural network (CNN) streams combined by the Dempster—Shafer (DS) model," *IEEE J. Sel. Topics Appl. Earth Observ. Remote Sens.*, vol. 14, pp. 452–463, Dec. 2020.

Haojie Cai received the B.S. degree in geoinformatics in 2018, from the China University of Geoscience, Wuhan, China, where he is currently working toward the M.S. degree in earth exploration and information technology.

His current research interests include landslide detection and remote sensing application.

Tao Chen (Senior Member, IEEE) received the Ph.D. degree in photogrammetry and remote sensing from Wuhan University, Wuhan China, in 2008.

From 2015 to 2016, he was a Visiting Scholar with the University of New South Wales, Sydney, NSW, Australia. He has authored or coauthored more than 40 scientific papers including IEEE JOURNAL OF SELECTED TOPICS IN APPLIED EARTH OBSERVATIONS AND REMOTE SENSING, *Remote Sensing*, *Environmental Earth Sciences*, and *Environmental Science and Pollution Research*. He is currently an Associate Professor with the Institute of Geophysics and Geomatics, China University of Geosciences, Wuhan, China. His research interests include image processing, machine learning, and geological remote sensing.

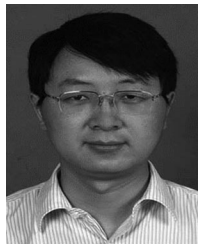

Ruiqing Niu received the Ph.D. degree in earth exploration and information technology from China University of Geosciences, Wuhan, China, in 2005.

He is currently a Full Professor with the Institute of Geophysics and Geomatics, China University of Geosciences, Wuhan, China. His research interests include remote sensing, geographic information system, and engineering geology.

Antonio Plaza (Fellow, IEEE) received the M.Sc. and Ph.D. degrees in computer engineering from the Department of Technology of Computers and Communications, University of Extremadura, Badajoz, Spain, in 1999 and 2002, respectively.

He is currently a Full Professor and the Head of the Hyperspectral Computing Laboratory, Department of Technology of Computers and Communications, University of Extremadura. He has authored or coauthored more than 600 publications and guest edited 10 journal special issues. He has reviewed more than 500 manuscripts for over 50 different journals.

Dr. Plaza served as the Editor-in-Chief for the IEEE TRANSACTIONS ON GEOSCIENCE AND REMOTE SENSING, from 2013 to 2017. He is included in the Highly Cited Researchers List (Clarivate Analytics), from 2018 to 2020.